ACS Catalysis

Research Article

pubs.acs.org/acscatalysis

Catalytic Efficiency Is a Function of How Rhodium(I) (5 + 2) Catalysts Accommodate a Conserved Substrate Transition State Geometry: Induced Fit Model for Explaining Transition Metal Catalysis

Thomas J. L. Mustard,[†] Paul A. Wender,*[,‡] and Paul Ha-Yeon Cheong*[,†]

[†]Department of Chemistry, Oregon State University, 153 Gilbert Hall, Corvallis, Oregon 97331-4003, United States

[‡]Departments of Chemistry and Chemical and Systems Biology, Stanford University, Stanford, California 94305-5080, United States

Supporting Information

ABSTRACT: The origins of differential catalytic reactivities of four Rh(I) catalysts and their derivatives in the (5 + 2) cycloaddition reaction were elucidated using density functional theory. Computed free energy spans are in excellent agreement with known experimental rates. For every catalyst, the substrate geometries in the transition state remained constant (<0.1 Å RMSD for atoms involved in bond-making and -breaking processes). Catalytic efficiency is shown to be a function of how well the catalyst accommodates the substrate transition state geometry and electronics. This shows that the induced fit model for explaining biological catalysis may be relevant to transition metal catalysis. This could serve as a general model for understanding the origins of efficiencies of catalytic reactions.

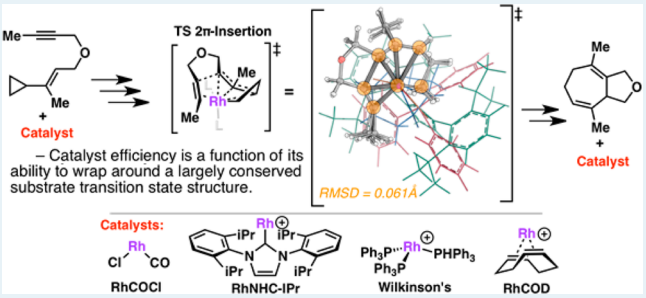

KEYWORDS: *DFT, transition metals, catalysis, organometallic, computations, theory, ligands, NHC, phosphine, rhodium*

1. INTRODUCTION

The design or discovery of new transition metal-catalyzed cycloaddition reactions is of preeminent importance to the realization of practical, atom-[1] and step-economical,[2] and green syntheses of compounds that exhibit significant biological activity and therapeutic potential;[3] however, the specific origins of different efficiencies of various transition metal cycloaddition catalysts remain elusive. For example, various Rh(I) catalysts are known to catalyze the (5 + 2) cycloaddition of vinylcyclopropanes (VCPs) to π-systems with a wide range of efficiencies (Table 1), but their differential reactivities remain poorly understood.[4,5] Herein, we disclose that the catalytic barriers for these (5 + 2) reactions are almost entirely dictated by the ability of the catalysts to geometrically and electronically conform around a conserved, rigid substrate transition state geometry. The surprising extent to which the substrate transition structure (TS) geometry is invariant to widely differing catalyst electronic and steric factors has direct practical implications on how catalysis can be understood and improved through rational design.

2. METHOD

All intermediates and transition states along the reaction coordinates for all four catalysts and derivatives were computed with density functional theory, M06//B3LYP, and the 6-31G* and LANL2DZ basis sets.[6] Interestingly, geometry optimizations with dispersion corrections (B3LYP-D3) or single points with triple-ζ basis sets (M06/def2-TZVP) led to erratic and uniformly worse agreements with experimental barriers.[7] Distortion-interaction energies[8] were computed for all structures. The distortion energies quantify the energetic

Table 1. Catalytic Efficiencies of Four Rh (5 + 2) Catalysts

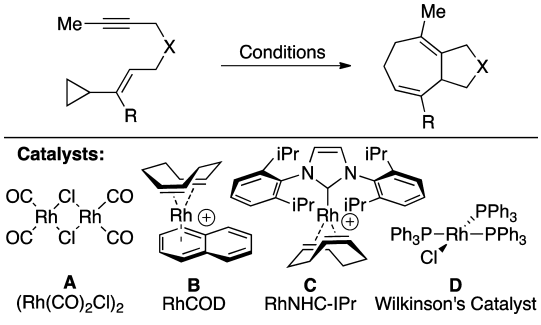

X	R	catalyst	conditions	TOF[a]	ΔG_{FES}
$C(CO_2Et)_2$	H	5 mol % **A**	110 °C, 20 min, 82%	1.0	26.5
$C(CO_2Et)_2$	H	2 mol % **B**	rt, 15 min, >99%	4.1	20.8
NTs	H	5 mol % **B**	rt, 65 min, 90%	1.0	20.8
NTs	H	2 mol % **C**	rt, 10 min, 93%	16.8	19.5
O	Me	10 mol % **D**	110 °C, 1020 min, 78%	1.0	38.5
O	Me	5 mol % **A**	110 °C, 20 min, 78%	102.0	26.5

[a]TOF = relative catalytic turnover over frequency.

Received: November 17, 2014
Revised: January 22, 2015
Published: January 27, 2015

DOI: 10.1021/cs501828e
ACS Catal. 2015, 5, 1758−1763

penalty of distorting the catalyst and substrate to reach the transition state geometry. Interaction energies quantify the electronic stabilization between the catalyst and substrate in the transition state.

3. RESULTS AND DISCUSSION

The complete reaction coordinates for the (5 + 2) cycloaddition of four archetypal Rh(I) catalysts were computed (Scheme 1): **A**, $(Rh(CO)_2Cl)_2$; **B**, Rh(COD)Naph$^+$ (COD = cyclooctadiene); **C**, Rh bis(2,6-diisopropylphenyl)-N-heterocyclic carbene (RhNHC-IPr; NHC-IPr = *N*,*N*′-(2,6-diisopropylphenyl)dihydroimidazolium); **D**, Wilkinson's catalyst. The mechanism of Rh (5 + 2) cycloaddition involving an alkyne and vinyl cyclopropane has been studied computationally (Scheme 1).[9] The catalytic cycle begins with the substrate−catalyst complex **I**, followed by oxidative ring opening of the VCP **TS-II**. The coordination of the 2π-alkyne **III** and subsequent 2π-insertion of **TS-IV** lead to the metallacycle intermediate **V**. Reductive elimination **TS-VI** forms the second C−C bond and leads to the product−catalyst complex **VII**. Transfer of the catalyst to another substrate releases the product and regenerates the catalyst.

Scheme 1. Mechanism of the Rh (5 + 2) Cycloaddition

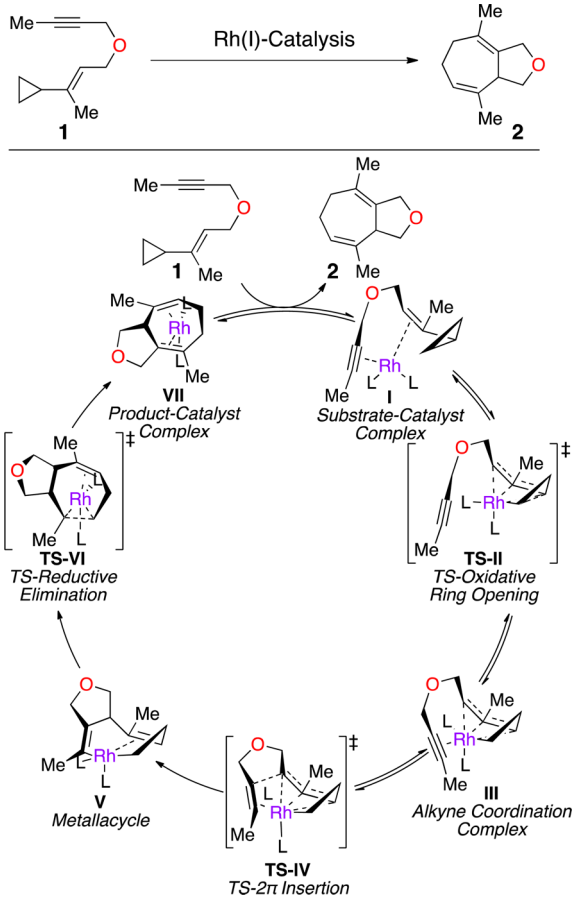

The computed reaction coordinate diagram for all catalysts is shown in Figure 1. The catalytic efficiency is directly proportional to the free energy span (FES) in the computed reaction coordinate with tethered vinylcyclopropane−alkyne **1**.[9b] The computed relative free energy spans and the observed relative catalytic efficiencies of four Rh (5 + 2) catalysts are in good agreement (Table 1). The RhCOD and RhNHC-IPr catalysts are the fastest, with a FES of 20.8 and 19.5 kcal/mol, respectively. The $(Rh(CO)_2Cl)_2$ catalyst with a FES of 26.5 is much slower, and Wilkinson's catalyst with a FES of 38.5 kcal/mol trails behind even more significantly.

The 2π-insertion and reductive elimination steps are of key interest in this reaction; the oxidative ring opening is known to be facile.[9a] The computed transition structures (TSs) involving all four catalysts for these two steps are shown in Figure 2. The geometries of the substrate are indistinguishable from each other: the atoms involved in the bond-forming and -breaking processes of 2π-insertion and reductive elimination transition states (highlighted in orange) share a root-mean-square deviation (RMSD) of 0.061 and 0.056 Å, respectively. The remarkable conservation of the substrate geometry in the transition states strongly suggests that the onus of reaching the transition state falls on the catalyst's ability to mitigate the electronic and steric effects presented by the substrate transition state geometry. This further suggests that the orbital geometries and preferences in the bond-breaking and -forming processes do not change between catalysts. These observations are consistent with the induced fit model for explaining biological catalysis. Similarly, all the catalysts appear to share the same behaviors in ligation preferences. A remarkably strong trans effect is seen in all key TSs. These preferences facilitate the reactivity of the metal center by either donating or removing electron density trans to the bond-forming or -breaking process as needed.

Catalyst A: $(Rh(CO)_2Cl)_2$. This neutral catalyst is an effective catalyst for the Rh (5 + 2) cycloaddition (ΔG_{FES} = 26.5 kcal/mol) (Figure 1). The minimal steric encumbrance of this catalyst all but eliminates catalyst distortion, and this correspondingly leads to low barriers for all key transition states (Figure 3); however, the transfer of catalyst from product to the next substrate is significantly endergonic (6.4 kcal/mol). We hypothesize that steric encumbrance in other catalysts typically aids in product release from the catalyst via a strain release.[10] Because the steric encumbrance of this catalyst is minimal, this process is more difficult.

Catalyst B: RhCOD. The cationic RhCOD has a significantly lower FES of 20.8 kcal/mol (Figure 1). The cyclooctadiene (COD) ligand stays in the twist-boat configuration throughout the catalytic cycle in order to maintain double ligation to Rh (Figure 3). The greater steric encumbrance of the COD ligand (in comparison with catalyst **A**) increases the catalyst distortion throughout the catalytic cycle. Despite this, the RhCOD maintains excellent catalysis as a result of two effects: (i) the product inhibition for RhCOD is significantly smaller than $(Rh(CO)_2Cl)_2$ (2.4 kcal/mol vs 6.4 kcal/mol, respectively), and (ii) strong stabilizing electronic interactions provided by the COD ligand mitigates the energetic penalty from distortions.[11]

The increased magnitude of electronic stabilization provided by the RhCOD catalyst is surprising. We believe this stabilization occurs from the hemilability[12] of the COD ligand, allowing it to adjust ligand ligation to maximize stabilizing electronic interactions and minimize destabilization. For an example, during the 2π-insertion, the ethylene cis to the forming bond partially dissociates (Rh-$(C{=}C)_{cis}$ 2.8 Å vs Rh-$(C{=}C)_{trans}$ 2.2 Å), suggesting that coordination to the cis position in the 2π-insertion is not stabilizing, but also that the ligand in the trans position is critically important to catalysis of this step. Hemilability allows the catalyst to dynamically tune the electronics to best catalyze the step at hand.

DOI: 10.1021/cs501828e
ACS Catal. 2015, 5, 1758−1763

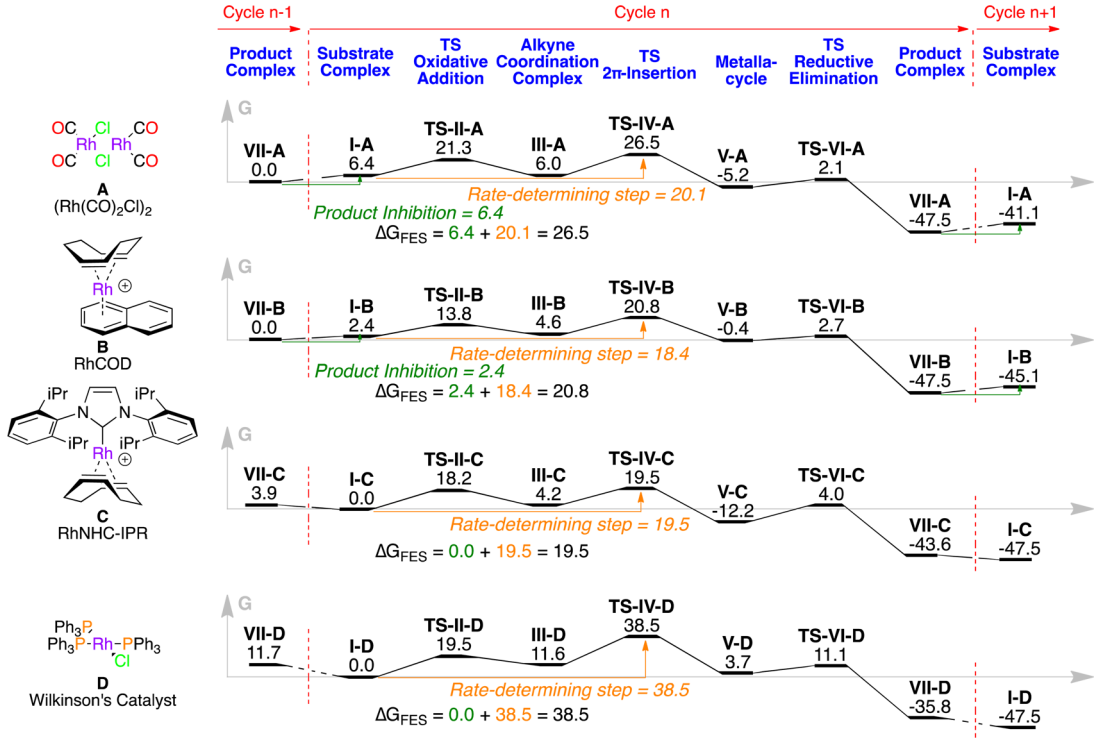

Figure 1. Computed reaction coordinate diagram involving substrate **1** and catalysts **A**, **B**, **C**, and **D** corresponding to Scheme 1.

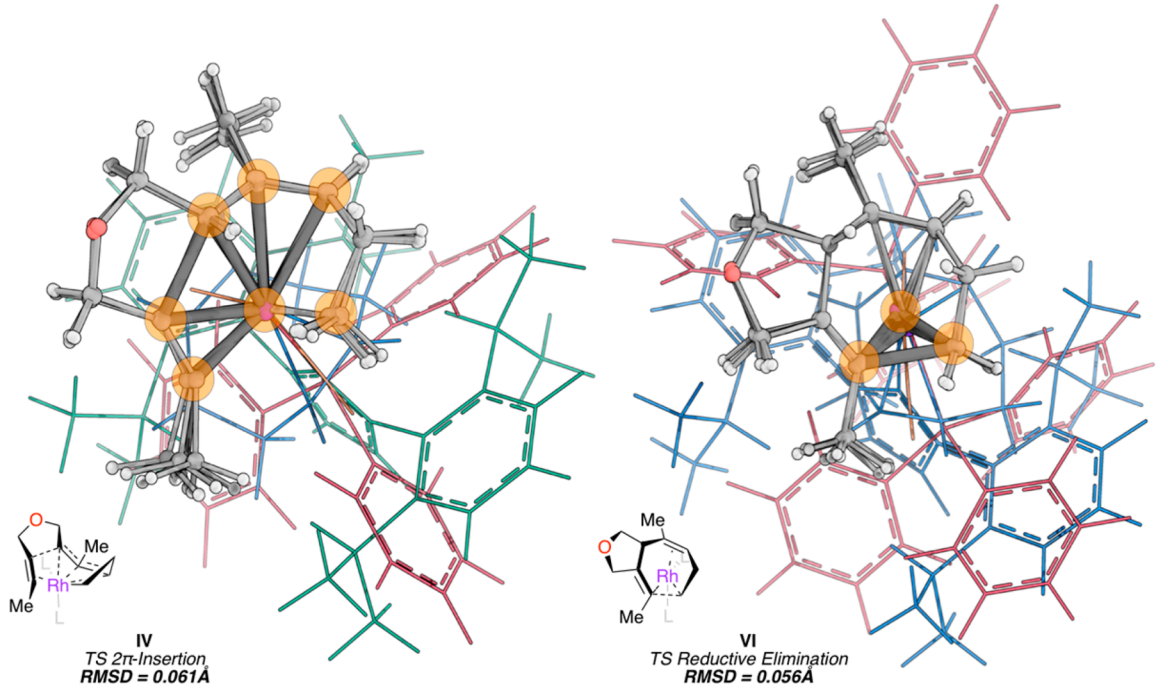

Figure 2. An overlay of four Rh(I)-catalysts. The substrate geometries in the transition structures are indistinguishable.[13] The atoms involved in the bond-forming and -breaking processes of 2π-insertion and reductive elimination transition state (highlighted in orange) share RMSDs of 0.061 and 0.056 Å, respectively.

To estimate the steric contributions to catalysis of the COD ligand, the reaction coordinate involving the smaller, untethered double diene catalyst, Rh diethylene (RhDiEt; DiEt = diethylene) (**E**, Figure 4.), was computed.[11] Three observations are substantive. First, the FES dropped to 14.6 kcal/mol as a result of the significantly increased stabilizing electronic interaction in the 2π-insertion step (116.9 vs 98.7 kcal/mol in the RhCOD). We attribute this to the greater flexibility with which the RhDiEt catalyst can further accommodate the electronic preferences of the substrate transition state. Second, the loss of the cis olefin amounts to negligible change in the 2π-insertion barrier ($\Delta\Delta G^{\ddagger}$ = 0.2 kcal/mol), reaffirming our hypothesis that the trans, not the cis geometry, is important for the stabilization of the 2π-insertion step. Last, the product inhibition of RhDiEt was found to be

DOI: 10.1021/cs501828e
ACS Catal. 2015, 5, 1758−1763

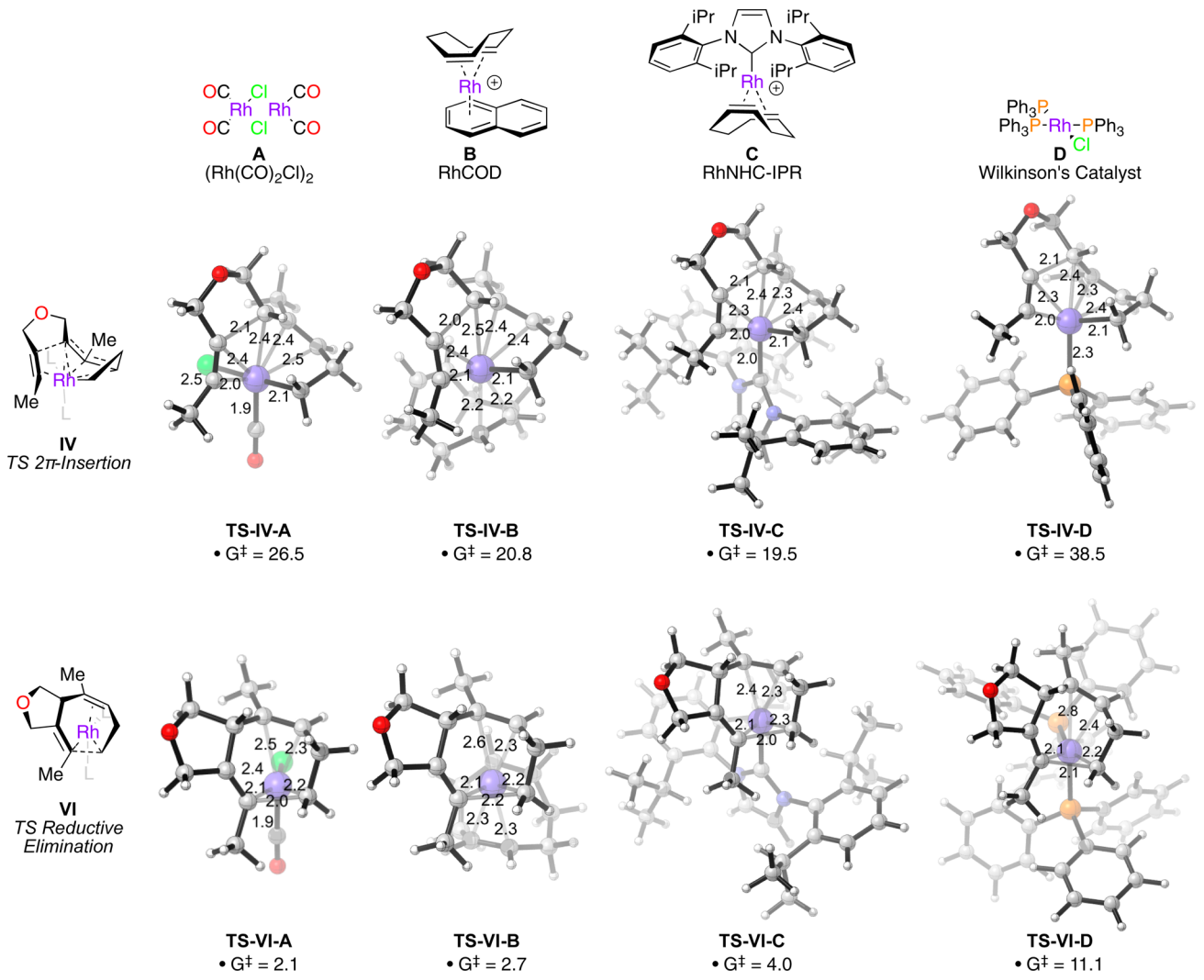

Figure 3. 2π-Insertion and reductive elimination transition structure involving substrate **1** and catalysts **A**, **B**, **C**, and **D**.[14]

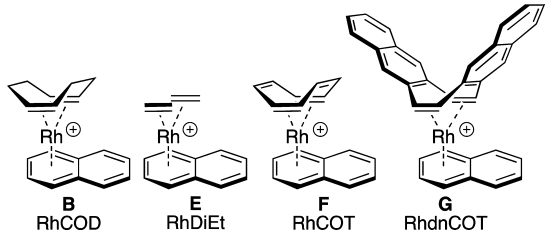

Figure 4. Rh cyclooctadiene (RhCOD) and derivatives: Rh diethylene (RhDiEt), Rh cyclooctatetraene (RhCOT), and Rh dinaphthylcyclooctatetraene (RhdnCOT).

equivalent to RhCOD (2.2 vs 2.4 kcal/mol, respectively). The distortions in the product−catalyst complex were also similar (27.9 vs 28.7 kcal/mol for the RhCOD), stemming from the steric interactions between the olefin hydrogens and the substrate/product. This increased steric encumbrance of the COD ligand as compared with the Rh dimer catalyst **A** aids in product extrusion to the tune of 4 kcal/mol; however, this does not completely eliminate product inhibition.

The electronic contributions of the tether were also studied for the Rh cyclooctatetraene (RhCOT; COT = 1,3,5,7-cyclooctatetraene) (**F**, Figure 4.) and Rh dinaphthylcyclooctatetraene (RhdnCOT; dnCOT = dinaphthyl-1,3,5,7-cyclooctatetraene) (**G**, Figure 4.) catalysts.[11] The increased interaction energy from the conjugated ligand system (as compared with RhCOD) lowered the energies for each state along the reaction coordinate. The FES of RhCOT and RhdnCOT dropped to 18.6 and 17.4 kcal/mol respectively (from 20.8 kcal/mol for RhCOD, **B**), yet product inhibition increased to 2.5 and 3.2 kcal/mol, respectively. We hypothesize that the change in hybridization of the tether from sp^3 to sp^2 leads to an increase in electronegativity, strengthening the electron-withdrawing abilities of the catalyst. These subtle but substantive changes for the RhCOD family of catalysts suggest that select perturbation of the tether geometry could lead to substantive increase in the catalytic efficiency of the Rh (5 + 2) process by eliminating product inhibition due to increasing steric bulk and increasing electronic stabilization by adding electron-withdrawing groups.

Catalyst C: RhNHC-IPr. The RhNHC catalyst exhibited the lowest FES of 19.5 kcal/mol (Figure 1). There are three origins for the notable efficacy of this catalyst. First, key agostic interactions between the Rh and the hydrogens of the diisopropyl groups on the bis-2,6-diisopropyl-N-heterocyclic carbene are found in transition structures (the oxidative addition and the reductive elimination), as well as intermediates, along the reaction coordinate and are critical for the electronic stabilization of these structures (Figure 3).[11] Second, the catalyst distortion is

DOI: 10.1021/cs501828e
ACS Catal. 2015, 5, 1758−1763

surprisingly small; in fact, 2.4 kcal/mol lower for the rate-determining 2π-insertion step compared with RhCOD. Third, unlike the previous Rh (5 + 2) catalysts discussed, the RhNHC-IPr exhibits no product inhibition.

To quantify the effects of the NHC substituents on catalysis, the reaction coordinate involving the unsubstituted parent RhNHC-H_2 (NHC-H_2 = dihydroimidazolium) was also computed (**H**, Figure 5).[11] Three observations are substantive:

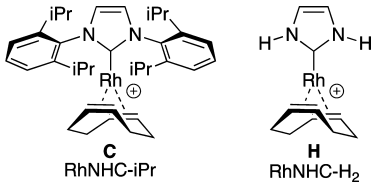

Figure 5. Rh *N,N′*-(2,6-Diisopropylphenyl)dihydroimidazolium (RhNHC-IPr) and Rh dihydroimidazolium (RhNHC-H_2).

first, the catalyst distortion of the small RhNHC-H_2 is nearly identical to the significantly larger RhNHC-IPr. This suggests that any distortion in the NHC-IPr is inherent within the NHC ligand, not with the substrate or Rh metal. Second, RhNHC-H_2 also shows no product inhibition. This strongly suggests that the lack of product inhibition in the RhNHC-IPr is not related to the steric repulsion between the large NHC-IPr ligand and the product. Third, the interaction energies between the catalyst and substrate were significantly different between the two ligands. The catalytic ability of NHC-IPr stems from its ability to manifest hemilability during the transition states. Agostic interactions in the NHC-IPr involving the aryl isopropyl C-Hs stabilized all transition structures where these interactions were geometrically possible and stabilizing. Notably, the oxidative addition and reductive elimination transition states were higher for the NHC-H_2 than the NHC-IPr (oxidative addition, 26.3 vs 18.2 kcal/mol; reductive elimination, 9.0 vs 4.0 kcal/mol, respectively). In the 2π-insertion transition step, there were no agostic interactions in RhNHC-IPr, presumably because of the steric congestion around the Rh center. In this case alone, RhNHC-H_2 had a lower barrier compared with the RhNHC-IPr (14.9 kcal/mol vs 19.5 kcal/mol).

Catalyst D: Wilkinson's Catalyst. The Wilkinson's catalyst, that is, tris-triphenylphosphine rhodium chloride (ClRhTPPh_3), has the highest FES of 38.5 kcal/mol (Figure 1). The ClRhTPPh_3 reaction is heterolobal. The catalytic cycles for the mono-, bis-, and tris-PPh_3 rhodium catalysts were computed. They differ considerably. The tris-PPh_3 Rh complex was found to be the resting state of the catalytic cycle and is catalytically inactive as a result of severe steric congestion (Figure 3). The steady state of this reaction begins with the unfavorable exchange of one of the triphenylphosphine (PPh_3) ligands with the substrate. The cycle continues in the bis-PPh_3 form through the oxidative addition to the 2π-complex. Another PPh_3 dissociates before the sterically congested 2π-insertion of TS. The subsequent metallacycle intermediate is most stable in the bis-PPh_3 form, and the reaction continues in this form through the reductive elimination and the product−catalyst complex. The product is released from the catalyst via the association of another PPh_3.

The 2π-insertion transition structure is the most sterically congested and electronically saturated (18-electron) structure along the reaction coordinate. In this transition state, the catalyst is in the mono-PPh_3 form, and the catalyst distortion is minimal. The energetic penalty of associating another PPh_3 is significant (38.5 vs 39.9 kcal/mol, respectively, for the mono and the bis).

It is critical to note that the reactivity in purely the bis- or mono-PPh_3 forms exhibits FESs of 30 and 16.9 kcal/mol, respectively.[11] The penalty for ligand exchange contributes significantly to the overall barrier for Wilkinson's catalyst. Dissociation of PPh_3 from the tris-PPh_3 resting state and substrate association is endergonic by 9.2 kcal/mol (Scheme 2). Thus, it would be entirely possible for less coordinationally saturated phosphine rhodium catalysts to be extremely reactive.[5k]

Scheme 2. Energetic Penalty of Dissociating PPh_3 To Associate Substrate Is 9.2 kcal/mol

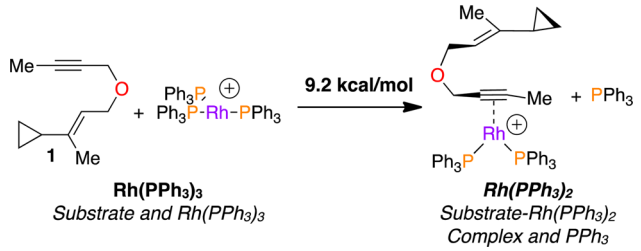

4. CONCLUSION

In conclusion, we have discovered that substrates in the transition states for Rh(I) catalyzed (5 + 2) cycloadditions are remarkably invariant with respect to structurally and electronically different catalysts. This suggests that the reactivities of Rh(I) catalysts are almost entirely dictated by the ability of the catalysts to geometrically and electronically conform around a conserved, rigid substrate, transition state geometry. This shows that the induced fit model for explaining biological catalysis may be relevant to transition metal catalysis. We suspect that this theme may be much more prevalent than previously suspected. Work is under way to identify if similar effects are present in other catalytic reactions. Last, our analysis of the four Rh (5 + 2) catalysts reveals the specific requirements to enhance each of these catalysts and lays the foundation for how transition metal catalysis can be improved through rational design.

■ ASSOCIATED CONTENT

Supporting Information

The following file is available free of charge on the ACS Publications website at DOI: 10.1021/cs501828e.

Computed structures, energies, thermodynamic corrections, distortion-interaction analyses, reaction coordinates, and more detailed figures of computed structures (PDF)

■ AUTHOR INFORMATION

Corresponding Authors

*E-mail: wenderp@stanford.edu.

*E-mail: paulc@science.oregonstate.edu

Notes

The authors declare no competing financial interest.

■ ACKNOWLEDGMENTS

P.H.-Y.C. is the Vicki & Patrick F. Stone Scholar of Oregon State University and gratefully acknowledges financial support from the Stone Family and the National Science Foundation (NSF, CHE-1352663). P.A.W. gratefully acknowledges support

DOI: 10.1021/cs501828e
ACS Catal. 2015, 5, 1758−1763

from the National Science Foundation (NSF, CHE1265956) and the National Institutes of Health (CA031845). T.J.L.M. and P.H.-Y.C. also acknowledge computing infrastructure in part provided by the NSF Phase-2 CCI, Center for Sustainable Materials Chemistry (NSF CHE-1102637). T.J.L.M. also acknowledges financial support from the N.L. Tartar Research Fellowship. T.J.L.M. and P.H.-Y.C. also acknowledge Ryne C. Johnston for assistance with the manuscript.

REFERENCES

(1) Trost, B. M. *Angew. Chem., Int. Ed.* **1995**, *34*, 259−281.
(2) (a) Wender, P. A.; Miller, B. L. *Nature* **2009**, *460*, 197−201. (b) Wender, P. A. *Nat. Prod. Rep.* **2014**, *31* (4), 433−440.
(3) (a) Kowalski, J. A. Ph.D. Thesis, Stanford University, Stanford, CA, 2005; pp 31−109. (b) He, W.; Cik, M.; Appendino, G.; Puyvelde, L. C.; Leysen, J. E.; De Kimpe, N. *Mini-Rev. Med. Chem.* **2002**, *2*, 185−200. (c) Borris, R. P.; Blasko, G.; Cordell, G. A. *J. Ethnopharmacol.* **1988**, *24*, 41−92. (d) Evans, F. J.; Soper, C. J. *Lloydia* **1978**, *41*, 193−233.
(4) (a) Wender, P. A.; Sperandio, D. *J. Org. Chem.* **1998**, *63*, 4164−4165. (b) Wender, P. A.; Williams, T. J. *Angew. Chem., Int. Ed.* **2002**, *41*, 4550−4553. (c) Lee, S. I.; Park, S. Y.; Park, J. H.; Jung, I. G.; Choi, S. Y.; Chung, Y. K. *J. Org. Chem.* **2006**, *71*, 91−96.
(5) For the first intramolecular and intermolecular examples, see: (a) Wender, P. A.; Takahashi, H.; Witulski, B. *J. Am. Chem. Soc.* **1995**, *117*, 4720−4721. (b) Wender, P. A.; Rieck, H.; Fuji, M. *J. Am. Chem. Soc.* **1998**, *120*, 10976−10977. for reviews, see: (c) Wender, P. A.; Gamber, G. G.; Williams, T. J. Rhodium(I)-Catalyzed [5 + 2], [6 + 2], and [5 + 2+1] Cycloadditions: New Reactions for Organic Synthesis. In *Modern Rhodium-Catalyzed Organic Reactions*; Evans, P. A., Ed.; Wiley-VCH: Weinheim, 2005; pp 263−299. (d) Pellissier, H. *Adv. Synth. Catal.* **2011**, *353*, 189−218. (e) Ylijoki, K. E.O.; Stryker, J. M. *Chem. Rev.* **2013**, *113*, 2244−2266. for more recent review, see: (f) Pellissier, H. *Adv. Synth. Catal.* **2011**, *353*, 189−218. (g) Wender, P. A. *Tetrahedron* **2013**, *69*, 7529−7550. (h) Schienebeck, C. M.; Li, X.; Shu, X.-Z.; Tang, W. *Pure Appl. Chem.* **2014**, *86*, 409−417. for more recent intramolecular and intermolecular examples, see: (i) Wender, P. A.; Fournogerakis, D. N.; Jeffreys, M. S.; Quiroz, R. V.; Inagaki, F.; Pfaffenbach, M. *Nat. Chem.* **2014**, *6*, 448−452. (j) Wender, P. A.; Inagaki, F.; Pfaffenbach, M.; Stevens, M. C. *Org. Lett.* **2014**, *16*, 2923−2925. (k) Wender, P. A.; Sirois, L. E.; Stemmler, R.; Williams, T. J. *Org. Lett.* **2010**, *12*, 1604−1607. (l) Wender, P. A.; Love, J. A.; Williams, T. J. *Synlett* **2003**, 1295−1298. (m) Gómez, F. J.; Kamber, N. E.; Deschamps, N. M.; Cole, A. P.; Wender, P. A.; Waymouth, R. M. *Organometallics* **2007**, *26*, 4541−4545. (n) Wender, P. A.; Lesser, A. B.; Sirois, L. E. *Angew. Chem., Int. Ed.* **2012**, *51*, 2736−2740. for intermolecular examples with no VCP, see: (o) Shu, X.-z.; Huang, S.; Shu, D.; Guzei, I. A.; Tang, W. *Angew. Chem., Int. Ed.* **2011**, *50*, 8153−8156. (p) Shu, X.-Z.; Schienebeck, C. M.; Song, W.; Guzei, I. A.; Tang, W. *Angew. Chem., Int. Ed.* **2013**, *52*, 13601−13605. (q) Shu, X.-z; Li, X.; Shu, D.; Huang, S.; Schienebeck, C. M.; Zhou, X.; Robichaux, P. J.; Tang, W. *J. Am. Chem. Soc.* **2012**, *134*, 5211−5221. (r) Schienebeck, C. M.; Robichaux, P. J.; Li, X.; Chen, L.; Tang, W. *Chem. Commun.* **2013**, *49*, 2616−2618.
(6) (a) B3LYP, B3LYP-D3, and M06 functionals with the 6-31G* (for H, C, N, O, P, and S) and LANL2DZ+ECP (for Rh and Br) or def2-TZVP (for all atoms) basis sets as implemented in Gaussian09 revision D.01. (b) Frisch, M. J.; Trucks, G. W.; Schlegel, H. B.; Scuseria, G. E.; Robb, M. A.; Cheeseman, J. R.; Scalmani, G.; Barone, V.; Mennucci, B.; Petersson, G. A.; Nakatsuji, H.; Caricato, M.; Li, X.; Hratchian, H. P.; Izmaylov, A. F.; Bloino, J.; Zheng, G.; Sonnenberg, J. L.; Hada, M.; Ehara, M.; Toyota, K.; Fukuda, R.; Hasegawa, J.; Ishida, M.; Nakajima, T.; Honda, Y.; Kitao, O.; Nakai, H.; Vreven, T.; Montgomery, J. A., Jr.; Peralta, J. E.; Ogliaro, F.; Bearpark, M.; Heyd, J. J.; Brothers, E.; Kudin, K. N.; Staroverov, V. N.; Kobayashi, R.; Normand, J.; Raghavachari, K.; Rendell, A.; Burant, J. C.; Iyengar, S. S.; Tomasi, J.; Cossi, M.; Rega, N.; Millam, M. J.; Klene, M.; Knox, J. E.; Cross, J. B.; Bakken, V.; Adamo, C.; Jaramillo, J.; Gomperts, R.; Stratmann, R. E.; Yazyev, O.; Austin, A. J.; Cammi, R.; Pomelli, C.; Ochterski, J. W.; Martin, R. L.; Morokuma, K.; Zakrzewski, V. G.; Voth, G. A.; Salvador, P.; Dannenberg, J. J.; Dapprich, S.; Daniels, A. D.; Farkas, Ö.; Foresman, J. B.; Ortiz, J. V.; Cioslowski, J.; Fox, D. J. *Gaussian 09, Revision D.01*; Gaussian, Inc.: Wallingford, CT, 2009. (c) Dahlke, E. E.; Olson, R. M.; Leverentz, H. R.; Truhlar, D. G. *J. Phys. Chem. A* **2008**, *112*, 3976. (d) Zhao, Y.; Truhlar, D. G. *Theor. Chem. Acc.* **2008**, *120*, 215.
(7) See the Supporting Information.
(8) For distortion/interaction theory examples, see: (a) Legault, C. Y.; Garcia, Y.; Merlic, C. A.; Houk, K. N. *J. Am. Chem. Soc.* **2007**, *129*, 12664−12665. (b) Liu, F.; Paton, R. S.; Kim, S.; Liang, Y.; Houk, K. N. *J. Am. Chem. Soc.* **2013**, *135*, 15642−15649.
(9) (a) Yu, Z.-X.; Wender, P. A.; Houk, K. N. *J. Am. Chem. Soc.* **2004**, *126*, 9154−9155. (b) Yu, Z.-X.; Cheong, P. H.-Y.; Liu, P.; Legault, C. Y.; Wender, P. A.; Houk, K. N. *J. Am. Chem. Soc.* **2007**, *130*, 2378−2379. (c) Liu, P.; Cheong, P. H.-Y.; Yu, Z.-X.; Wender, P. A.; Houk, K. N. *Angew. Chem.* **2008**, *47*, 3939−3941. (d) Liu, P.; Sirois, L. E.; Cheong, P. H.-Y.; Yu, Z.-X.; Hartung, I. V.; Rieck, H.; Wender, P. A.; Houk, K. N. *J. Am. Chem. Soc.* **2010**, *132*, 10127−10135. (e) Xu, X.; Liu, P.; Lesser, A.; Sirois, L. E.; Wender, P. A.; Houk, K. N. *J. Am. Chem. Soc.* **2012**, *134*, 11012−11025. (f) Xu, X.; Liu, P.; Shu, X.-Z.; Tang, W.; Houk, K. N. *J. Am. Chem. Soc.* **2013**, *135*, 9271−9274.
(10) (a) Schreiber, J.; Eschenmoser, A. *Helv. Chem. Acta* **1955**, *38*, 1529−1536. (b) Barton, D. H. R. *Experientia* **1950**, *6*, 316. (b) Barton, D. H. R. *J. Chem. Soc.* **1953**, 1027. (d) Rocek, J.; Westheimer, F. H.; Eschenmoser, A.; Moldoványl, L.; Schreiber, J. *Helv. Chem. Acta* **1962**, *45*, 2554−2567. (e) Wilcox, C. F., Jr; Sexton, M.; Wilcox, M. F. *J. Org. Chem.* **1963**, *28*, 1079−1082.
(11) The four catalysts and their derivatives' geometries, energies, thermodynamic corrections, agostic interactions, distortion−interaction analyses, and reaction coordinates can be found in the Supporting Information.
(12) (a) Miller, E. M.; Shaw, B. L. *Dalton Trans.* **1974**, *5*, 480−485. (b) Bader, A.; Lindner, E. *Coord. Chem. Rev.* **1991**, *108*, 27−110. (c) Jiménez, M. V.; Fernández-Tornos, J.; Pérez-Torrente, J. J.; Modrego, F. J.; Winterle, S.; Cunchillos, C.; Lahoz, F. J.; Oro, L. A. *Organometallics* **2011**, *30*, 5493−550. (d) Nomura, N.; Jin, J.; Park, H.; RajanBabu, T. V. *J. Am. Chem. Soc.* **1998**, *120*, 459−460.
(13) Computed structures rendered using Pymol. *The PyMOL Molecular Graphics System, version 1.3*; Schrödinger, LLC.
(14) Legault, C. Y. *CYLview, version 1.0b*; UCLA: Los Angeles, CA, 2007.

DOI: 10.1021/cs501828e
ACS Catal. 2015, 5, 1758−1763